Opt Quant Electron (2009) 41:735–749
DOI 10.1007/s11082-010-9386-y

Measurement and analysis of optical gain spectra in 1.6 to 1.8 μm InAs/InP (100) quantum-dot amplifiers

B. W. Tilma · M. S. Tahvili · J. Kotani · R. Nötzel · M. K. Smit · E. A. J. M. Bente

Received: 10 September 2009 / Accepted: 6 April 2010 / Published online: 4 May 2010
© The Author(s) 2010. This article is published with open access at Springerlink.com

Abstract Small signal modal gain measurements have been performed on two-section ridge waveguide InAs/InP (100) quantum-dot amplifiers that we have fabricated with a peak gain wavelength around 1.70 μm. The amplifier structure is suitable for monolithic active-passive integration, and the wavelength region and wide gain bandwidth are of interest for integrated devices in biophotonic applications. A 65 nm blue shift of the peak wavelength in the gain spectrum has been observed with an increase in injection current density from 1,000 to 3,000 A/cm^2. The quantum-dot amplifier gain spectra have been analyzed using a quantum-dot rate-equation model that considers only the carrier dynamics. The comparison between measured and simulated spectra shows that two effects in the quantum-dot material introduce this large blue shift in the gain spectrum. The first effect is the carrier concentration dependent state filling with carriers of the bound excited and ground states in the dots. The second effect is the decrease in carrier escape time from the dots to the wetting layer with decreasing dot size.

Keywords Semiconductor optical amplifiers · Quantum dots · Gain measurement · Rate equations · Integrated optoelectronics

Abbreviations

QD	Quantum dot
SOA	Semiconductor optical amplifier
CW	Continuous wave
WL	Wetting layer
ES	Excited state
GS	Ground state
PL	Photoluminescence

B. W. Tilma (✉) · M. S. Tahvili · J. Kotani · R. Nötzel · M. K. Smit · E. A. J. M. Bente
COBRA, Eindhoven University of Technology, Den Dolech 2, P.O. Box 513, 5600 MB Eindhoven, The Netherlands
e-mail: b.w.tilma@tue.nl

ASE	Amplified spontaneous emission
SE	spontaneous emission
MOVPE	Metal-organic vapor-phase epitaxy
SCH	Separate confinement heterostructure
FWHM	Full width half maximum

1 Introduction

The behavior of semiconductor quantum-dots (QDs) has extensively been studied over the last fifteen years. The use of QDs in monolithic optical devices, such as semiconductor optical amplifiers (SOAs) and semiconductor lasers, can have a number of benefits over the use of bulk or quantum well gain material. These advantages are due to the three dimensional carrier confinement in QDs. Some of the benefits that have been experimentally demonstrated are a comparatively low lasing threshold current density (Liu et al. 1999) and ultra fast gain recovery in optical amplifiers (Borri et al. 2000; Bogaart et al. 2005). Another major advantage of QDs over bulk or quantum well material is the wavelength tunability. The wavelength of a generated photon depends first of all on the discrete energy levels in the quantum dot and can only be changed a bit due to the temperature dependent homogeneous broadening (Sugawara et al. 1999). The discrete energy levels in the QD are however directly dependent on the size (and shape) of the dots (Holm et al. 2002) which means that the distribution of the size of the dots in an amplifier determines to a large extent the gain spectrum. In this paper we present results on InAs QD on an InP (100) substrate. The average QD size in this system can be controlled in the growth process which makes it possible to tune the average wavelength (Gong et al. 2004; Anantathanasarn et al. 2006; Nötzel et al. 2006). Most results that have been published up to now on this material are in the 1.55 μm telecom region where wide gain spectra (e.g. 80 nm wide) have been observed. However, the average dot size can also be tuned to end up with gain material which has a centre emission wavelength in the 1.70 μm region or even longer wavelength regions.

Such wavelengths in combination with a wide gain bandwidth are desirable for other applications such as tunable lasers for gas detection (Werle 1998) or optical coherence tomography (Fercher et al. 2003). This extension of the wavelength range of an amplifier structure that can be used in active-passive optical integration schemes (Bente and Smit 2006; Wang et al. 2008) opens up the possibility to develop integrated light sources for these applications.

In order to be able to optimally apply this gain material in devices for applications in these longer wavelength ranges, we have measured the small signal gain spectra of InAs/InP(100) ridge waveguide amplifiers as a function of injection current and modeled this QD material to understand its behavior. This can be utilized for instance for increasing the gain bandwidth of the optical amplifier by using multiple amplifier sections which are operated at different injection current densities (Xin et al. 2007).

In this paper we start with presenting the measurement method, the InAs/InP QD devices used and the characterization results in the 1.60–1.80 μm region. Then the QD amplifier model that was used to explain the dependency of the observed gain spectra on injection current is presented. The modeling of QD materials is more involved than the modeling of bulk or quantum well gain material due to the inhomogeneous character of the QD gain material. Extensive QD models have been presented especially for $In_xGa_{1-x}As/GaAs$ QD materials (Sugawara et al. 2000; Gioannini and Montrosset 2007) but also for InAs/InP QD materials (Grillot et al. 2009) Here we have simplified a commonly used QD amplifier model to calculate the small signal gain spectrum of the amplifiers and to fit a number of the

model parameters to the experimental data. Three important parameters are the electron-hole transition energies of the wetting layer (WL), the excited state (ES) and the ground state (GS). From InAs QD on GaAs substrate these transition energies can be determined with photoluminescence (PL) measurements or comparable measurement techniques. In these PL measurement results two individual peaks can be observed, one for the GS and one for the ES. PL measurements from InAs QD on InP substrate show however only one wide individual peak and no feature is observed that can be attributed to the wetting layer. The peaks from the GS and ES do overlap, which makes it impossible to extract the transition energies of the dots and the WL with this PL measurement technique (Allen et al. 2002; Caroff et al. 2005). Using the model we have been able to determine the transition energies of the GS and ES and an effective transition energy for the wetting layer.

The fitted results are discussed in the last section together with the explanation that was found for the large shift in peak wavelength in the gain spectrum with the change in injection current density.

2 Gain measurement method, device design and fabrication

Small signal gain spectra of optical amplifiers are often determined with the well known Hakki-Paoli technique (Hakki and Paoli 1975; Barbarin et al. 2006) In this method the optical gain is derived from the contrast ratio or shape of the modulations in the spectrum of the Amplified Spontaneous Emission (ASE) caused by the resonances of a laser cavity operating below threshold. Our quantum dot amplifiers have a relatively low modal gain and therefore need to be typically at least a few millimeters long to generate detectable signal. The spectral measurements therefore have to be done using a high resolution spectrometer in order to resolve the spectral modes and not to distort the observed contrast ratio and/or line width of the modes. Since such a high resolution spectrometer in the 1.60–1.80 μm wavelength region is not available to us we have used a measurement technique based on the analysis of ASE spectra from different lengths of amplifiers as described by (Oster et al. 1997; Thomson et al. 1999). By this method the gain can be calculated from the ASE spectra over a wide range of injection current densities.

Under the condition that there is no optical feedback and there is no gain saturation in the amplifier, the net modal gain G of a semiconductor optical amplifier (SOA) of length L is related to its ASE output power P according to (Thomson et al. 1999):

$$P = \frac{P_{sp}}{G}\left(e^{GL} - 1\right) \tag{1}$$

where P_{sp} is the spontaneous emission (SE) power (per unit length) and L is the SOA length. Note that the net modal gain G relates to the material gain g according to: $G = \Gamma g - \alpha_i$. Where Γ is the optical confinement factor and α_i is the internal loss. Note that this loss value is generally quite high for SOAs, in the order of 10–20 cm^{-1}. We have extracted the gain by using the ASE spectra from a series of amplifiers of different lengths at constant current density and fitting Eq. (1) on the data at each wavelength to extract the parameters G and P_{sp}. This fitting has several advantages over using only two lengths (L and $2L$) as presented by (Thomson et al. 1999) to extract the gain. First of all, the different ASE spectra always contain noise or small deviations in comparison to the ideal situation described by Eq. (1). These deviations will be averaged out by the fitting over multiple devices. Secondly, measurement points that deviate over 10% from the expected value on the curve are detected easily. Such points were found to deviate due to misalignment or fabrication imperfections. When

this is observed at one current setting for one device, it turned out there was an alignment issue and a new measurement was done which typically resulted in a measurement point close to the curve formed by the other points. When such a large deviation is observed at all current settings on one particular device, we have concluded that the device is not working properly, most probably due to fabrication imperfections. Measurements from such devices were excluded from further analysis.

We have realized a chip with a series of parallel amplifiers with different lengths that have two contact sections. One of the two sections is forward biased to produce the ASE and the second section is reverse biased in order to absorb the ASE from the first section to prevent any significant feedback which is particularly important when using this method. The ratio of the length of the amplifier and absorber sections is varied so the different lengths of amplifiers are realized on a single chip.

This series of two-section ridge waveguide amplifiers was realized on a single chip starting from the QD gain material grown on an n-type InP (100) substrate by metal-organic vapor-phase epitaxy (MOVPE), as presented in (Anantathanasarn et al. 2006). In the active region, five InAs QD layers are stacked with an ultrathin GaAs interlayer underneath each QD layer to control the size of the QDs. These QD layers are placed in the center of a 500 nm InGaAsP (Q1.25) optical waveguiding core layer. The QD layers are designed to produce a gain spectrum in the 1.60–1.80 μm wavelength region. The bottom cladding of these devices is a 500 nm thick n-InP buffer and the top cladding is a 1.5μm p-InP layer with a compositionally graded 300 nm p-InGaAs(P) top contact layer. This layer stack is compatible with a butt-joint active-passive integration process for possible further integration (Wang et al. 2008). The single (lateral) mode 2μm wide ridge waveguides are etched 100 nm into the InGaAsP waveguiding layer using an optimized CH_4/H_2 two step reactive-ion dry etch process. To achieve electrical isolation between the two sections, the most highly doped part of the p-cladding layer is etched away between the two sections. The structures are planarized using polyimide. Two evaporated (TiPlAu) and plated (Au) metal pads contact the two sections to create two contacts. The backside of the n-InP substrate is metalized to create a common ground contact for the two sections. The structures are cleaved perpendicularly to the waveguide ridge, and no coating was applied. Finally the devices are mounted on a copper chuck, pside up and contacted with a probe.

The results presented in this paper have been obtained from 22 out of 26 two-section ridge waveguide devices with a total length of 7 mm. Four devices could not be used due to damage during fabrication or measurements. All devices are parallel on a single chip and are separated from each other by 250μm. The absorber section in different devices comprises between 5% and 30% of the total ridge length, and is separated from the amplifier section with an isolation section. Therefore, the length of the amplifiers would be 6.48–4.94 mm.

3 Gain measurement results

The QD amplifier gain spectrum has been determined by first measuring the continuous wave (CW) amplified spontaneous emission (ASE) with different injection current densities while keeping the temperature constant (288 K). The long section is used to inject a current which is adjusted to get a certain injection current density. On the smaller section of the ridge waveguide a -3 V reverse bias voltage is applied to work as an absorber and so prevent optical feedback. The single-pass amplified spontaneous emission generated in the QD ridge amplifiers was collected with a lensed fiber and the spectrum recorded with a 0.5 nm resolution spectrometer over 300 nm in 3,000 data points. As an example, in Fig. 1a

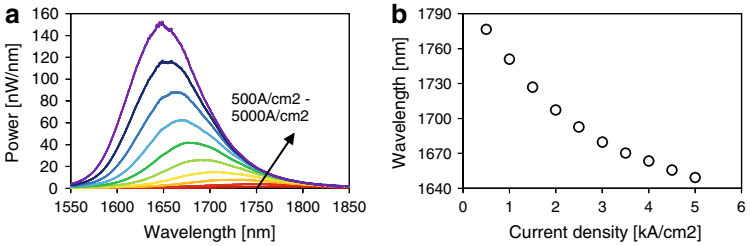

Fig. 1 **(a)** ASE spectrum from the 4.97 mm amplifier section under different injection current densities between 500 and 5,000 A/cm^2 in steps of 500 A/cm^2. **(b)** Peak wavelength of the ASE spectrum from the 4.97 mm amplifier with respect to the injection current density

the recorded ASE spectra for a 4.97 mm amplifier section are given for injection current densities between 500 and 5,000 A/cm^2. From this figure we observe a 130 nm shift in the peak wavelength as a function of the injection current density from 1.778 μm at 500 A/cm^2 to 1.649 μm at 5,000 A/cm^2. In Fig. 1b the peak wavelengths with respect to the injection current density are given. Note that in these figures no clear spectral features can be observed that could be identified with ASE from specifically the GS, the ES or any other higher energy state even at the highest current density (5 kA/cm^2). In measured ASE spectra from InAs QD on GaAs the separation between GS and ES can clearly be seen. In these spectra two different peaks can be distinguished at high injection currents, one for the GS and one for the ES.

To determine the gain spectra, the ASE is measured for 22 amplifier lengths and 5 injection current densities. Injection current densities above 3 kA/cm^2 could not be used with the available devices due to the fact that the absorber started to be bleached at these injection current densities and optical feedback started to occur. At all injection current densities used this feedback could be neglected. To ensure that the feedback through the absorber is negligible we did measure the optical spectrum from the absorber side output. By comparing the amplifier output spectrum and the absorber output spectrum we were able to determine the total roundtrip gain and the fraction of amplifier output signal originating from the feedback through the absorber. For the most unfavorable combination of amplifier current density and absorber length used (3 kA/cm^2, 730 μm) the wavelength dependent roundtrip gain was at most -18 dB at the most unfavorable wavelength. This means that less than 2% of the recorded power at that wavelength is caused by the back reflection under the most unfavorable circumstances used. The total amount of light which comes back in the amplifier through the absorber was determined to be -49 dBm. Furthermore, injection current densities below 1 kA/cm^2 could not be used due to the low signal level. A nonlinear least square algorithm fitting algorithm was used to fit the parameters in Eq. (1) to the data. In Fig. 2 the measured ASE power versus the length of the amplifiers is given for situations with a high gain (a), intermediate gain (b) and weak absorption (c). In the figures also the 10% error bars of the ASE measurements are given as well as the fitted gain curves. For each wavelength channel a weighted fit is made on the recorded power data for one wavelength over up to 22 different amplifier lengths and the zero length data point. For this zero length data point the dark spectrum of the spectrum analyzer is used which is approximately -75 dBm/nm over the full bandwidth. The weighting factor for the data points including the zero point is $W_i = 1/\left((\varepsilon \cdot P_i)^2 + \sigma_d^2\right)$, where $\varepsilon = 0.1$ is the relative error estimate and σ_d is the standard deviation of the dark spectrum of the spectrum analyzer. The influence of including the zero point is small. The fitting without the zero data point resulted in a slightly higher (less than 10%) gain value but the same spectral

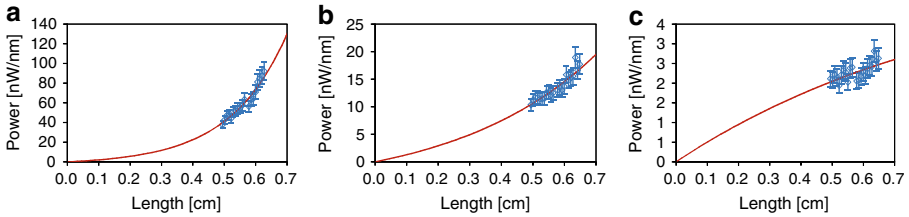

Fig. 2 Recorded ASE power versus amplifier length, the 10% *error bars* and the *fitted curve*. **(a)** $\boldsymbol{\lambda} = 1.70\,\mu\text{m}$, $\mathbf{I} = 3{,}000\,\text{A/cm}^2$, $\mathbf{G}_{\text{fit}} = 5.54\text{cm}^{-1}$ and 19 data points (The 3 longest amplifiers could not be used due to the presence of feedback in the ASE spectrum). **(b)** $\boldsymbol{\lambda} = 1.75\,\mu\text{m}$, $\mathbf{I} = 2000A/\text{cm}^2$, $\mathbf{G}_{\text{fit}} = 2.24\text{cm}^{-1}$ and 22 data points. **(c)** $\boldsymbol{\lambda} = 1.64\,\mu\text{m}$, $\mathbf{I} = 1{,}500\,\text{A/cm}^2$, $\mathbf{G}_{\text{fit}} = -1.07\text{cm}^{-1}$ and 22 data points

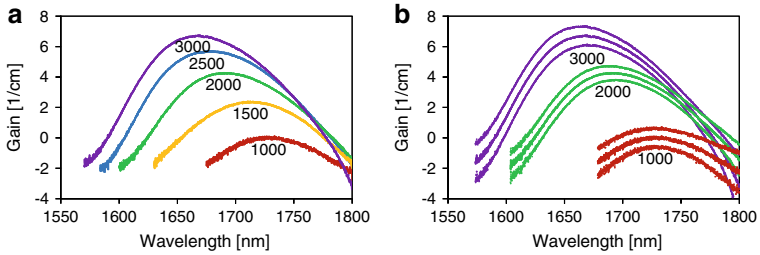

Fig. 3 **(a)** Modal gain spectra determined from measured ASE spectra for different injection current densities between 1,000 and 3,000 A/cm^2 **(b)** Selected model gain spectra including the 68% confidence bounds

shape. Besides the gain parameter also the spontaneous emission power (per unit length) P_{sp} is extracted at each wavelength from the fitting. In Fig. 3a the modal gain spectra which are determined from the ASE spectra with the fittings are given for the different injection current densities. Figure 3b shows the 68% confidence bounds for three of the derived gain curves. Note that this measurement technique is not suitable for absorption measurements due to the low signal level from attenuated ASE far from output of the amplifier. Obviously a similar blue shift with increasing injection current density is observed.

The shift in peak wavelength with current density is the most notable aspect of what we have observed in the gain spectrum. In practice it means that when this material is used in a laser without wavelength selective devices, e.g. a simple Fabry-Pérot laser, the lasing wavelength is strongly dependent on the length of the device. The longer the laser, the lower the gain per unit length or the lower the injection current density needs to be, and thus the laser will operate at a significantly longer wavelength then one that is say twice as short. A similar effect also occurs with quantum well or bulk gain material but we found it is more significant in the InAs/InP quantum dot materials. The shift in the peak of the gain spectrum due to temperature changes is relatively small and has been observed to be approximately 1 nm per degree K. No change in shape of the gain spectrum was observed over a range of 20 degrees at constant current density.

4 Quantum dot amplifier gain model

To understand the origin of the shape and in particular the blue-shift of the gain spectrum with increasing injection current density in our amplifiers, we have set up a simulation of the QD amplifier gain with a QD rate equation model as presented in (Sugawara et al. 2000;

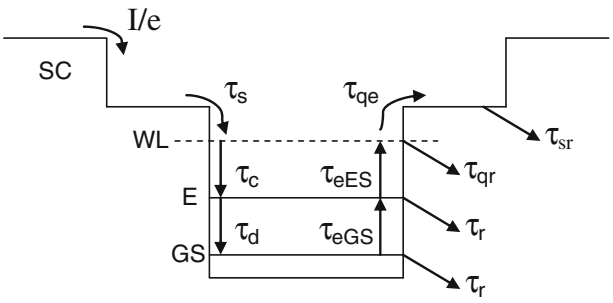

Fig. 4 Schematic op the energy band diagram of the QD amplifier active region. The carrier capture and escape rates from the various states are indicated

Gioannini and Montrosset 2007) which has been simplified for our purpose to reduce the calculation time. In this model we assume that the dots are neutral in electrons and holes since there is no doping in the dots. We treat an electron and a hole as an exciton and assume that the dynamics are controlled by the electron and that the hole immediately follows. We therefore use the same time constants for electrons and holes for the relaxation processes as well as the escape and recombination processes. The energy states of the hole in the dots and in the WL are assumed to be equal and are used as zero energy reference level. In this paper we use electron energy levels in the calculations which are equal to the transition energy values because of the zero reference level of the holes. The carrier losses in the dots due to stimulated emission were neglected because we only look at the low power ASE spectra far below the lasing threshold. Therefore we did not include a series of equations for the photons, which reduces the number of equations to be solved by nearly one third. In the model the homogeneous and inhomogeneous broadening are taken into account as well as the occupation dependent capture times and temperature and energy level dependent escape times. Also we did not include the Auger effect (Grillot et al. 2009) or any other many body effects, and no direct relaxation from WL to GS (Grillot et al. 2009) or any other higher energy states in the dots (Rossetti et al. 2008). Inclusion of these aspects would significantly increase the number and complexity of the equations and increase calculation times too much. Including direct relaxation from the WL to the GS in the model using values reported in literature (Miska et al. 2009) does not significantly influence the results from the model.

A schematic picture of the dynamics in the QD amplifier gain model is given in Fig. 4. The model describes a separate confinement heterostructure (SCH) where the carriers are injected and a WL that acts as a common carrier reservoir for the QDs. To include the inhomogeneous dot size distribution, the ES and the GS of the QDs are allocated into N sub groups, each represent a different average dot size with a different average ES and GS energy level. The dot size distribution is assumed to be Gaussian (Sugawara et al. 2000) with a full-width-half-maximum (FWHM) of Γ_0 and with G_n being the fraction of the n-th dot group. Carriers are injected in the SCH layer with a constant rate I/e. From this SCH layer they can relax to the WL with rate $1/\tau_s$. Carriers which are in the WL are able to escape back to the SCH layer with a rate $1/\tau_{qe}$ or can be captured into a QD from the nth subgroup with a rate $1/\tau_c$ which is dependent on the average capture time from the WL to the ES $1/\tau_{c0}$ assuming an empty ES, and dependent on the filling probability P_{ESn} of the ES. In the ES the carriers can escape back to the WL with a rate $1/\tau_{eESn}$ or can relax to the GS of the dot with a rate $1/\tau_d$ which is dependent on the average capture time from the ES to the GS $1/\tau_{d0}$ assuming an empty GS, and dependent on the filling probability P_{GSn} of the GS. From the GS the carriers can

escape back to the ES with a rate $1/\tau_{eGSn}$. Carriers can also recombine through radiative and non-radiative processes from the SCH, the WL and the two energy states in the dots with a rate $1/\tau_{sr}$, $1/\tau_{qr}$ and $1/\tau_r$ respectively.

The resulting rate equation system is as follows:

$$\frac{dN_s}{dt} = \frac{I}{e} - \frac{N_s}{\tau_s} - \frac{N_s}{\tau_{sr}} + \frac{N_q}{\tau_{qe}}, \tag{2}$$

$$\frac{dN_q}{dt} = \frac{N_s}{\tau_s} + \sum_n \frac{N_{ESn}}{\tau_{e_{ESn}}} - \frac{N_q}{\tau_{qr}} - \frac{N_q}{\tau_{qe}} - \frac{N_q}{\tau_{c0}} \sum_n (1 - P_{ESn})\, G_n, \tag{3}$$

$$\frac{dN_{ESn}}{dt} = \frac{N_q G_n\,(1 - P_{ESn})}{\tau_{c0}} + \frac{N_{GSn}\,(1 - P_{ESn})}{\tau_{e_{GSn}}} - \frac{N_{ESn}}{\tau_r} - \frac{N_{ESn}}{\tau_{e_{ESn}}} - \frac{N_{ESn}}{\tau_{d0}}\,(1 - P_{GSn}), n = 0, 1, ..., N - 1, \tag{4}$$

$$\frac{dN_{GSn}}{dt} = \frac{N_{ESn}}{\tau_{d0}}\,(1 - P_{GSn}) - \frac{N_{GSn}}{\tau_r} - \frac{N_{GSn}\,(1 - P_{ESn})}{\tau_{e_{GSn}}}, n = 0, 1, \ldots, N - 1, \tag{5}$$

The rate equation systems consists of a series of rate-equations (2, 3, 4, 5) which represent the total number of carriers in the SCH reservoir N_s, the total number of carriers in the WL reservoir N_q, and two series of N rate-equations which represent the carriers in the ES of the n-th dot group N_{ESn} and the carriers in the GS of the n-th dot group N_{GSn}. The carrier escape time τ_{eGSn} and τ_{eESn} from the GS to the ES and the ES to the WL respectively are according to the principle of detailed balance related to the carrier capture time τ_{d0} and τ_{c0} in the following way:

$$\tau_{e_{GSn}} = \tau_{d0} \frac{\mu_{GS}}{\mu_{ES}} e^{\frac{E_{ESn} - E_{GSn}}{k_B T}}, n = 0, 1, \ldots, N - 1, \tag{6}$$

$$\tau_{e_{ESn}} = \tau_{c0} \frac{\mu_{ES} N_D A_D}{\rho_{WL_{eff}} A_{WL}} e^{\frac{E_{WL} - E_{ESn}}{k_B T}}, n = 0, 1, \ldots, N - 1, \tag{7}$$

where $\mu_{GS}=2$ and $\mu_{ES}=4$ are the degeneracy of the GS and the ES levels; E_{WL}, E_{ESn} and E_{GSn} are the electron energy levels of the WL and the n-th ES and GS; N_D the dot density; ρ_{WLeff} the effective density of states in the WL; A_D the total area of the QD amplifier active region and A_{WL} the total area of the WL. $N_D A_D$ is in (7) the total number of dots in the amplifier and $\rho_{WLeff} A_{WL}$ the total number of effective states in the WL. A_D and A_{WL} have the same value.

The coupled rate equations have been solved in the time domain with a solver based on the second order modified Rosenbrock formula (Rosenbrock 1963). The set of equations are integrated in time till a steady state has been reached. From this situation the gain from different dots to the optical spectrum, which has been divided in M spectral groups, has been calculated with the equations:

$$g_{mn_{GS}} = \mu_{GS} C_g \frac{N_D}{N_W H_{act}} \frac{\left|P^{\sigma}_{GS}\right|^2}{E_{GSn}} (2P_{GSn} - 1)\, G_n B_{cv}\, (E_m - E_{GSn}), \tag{8}$$

$$g_{mn_{ES}} = \mu_{ES} C_g \frac{N_D}{N_W H_{act}} \frac{\left|P^{\sigma}_{ES}\right|^2}{E_{ESn}} (2P_{ESn} - 1)\, G_n B_{cv}\, (E_m - E_{ESn}), \tag{9}$$

where g_{mnGS} and g_{mnES} are the contribution to the gain from the n-th dot group to the m-th spectral mode from the GS and the ES respectively. $C_g = \pi e^2 \hbar / c n_r \varepsilon_0 m_0^2$ is a constant; N_W is the number of QD layers; H_{act} is the average active quantum dot layer thickness; $|P^{\sigma}_{GS,ES}|^2$

Table 1 Used parameter values

Simulation parameter	Value	Reference
FWHM of inhomogeneous broadening	$\Gamma_0 = 41$ meV	(Bogaart et al. 2005)
Effective density of states in the WL	$\rho_{\mathrm{WLeff}} = 2.4 \cdot 10^{11}\mathrm{cm}^{-2}$ ($T = 288$ K)	
FWHM of Homogeneous broadening	$2\hbar\Gamma_{\mathrm{cv}} = 40$ meV	Fit
Degeneracy of the GS	$\mu_{\mathrm{GS}} = 2$	
Degeneracy of the ES	$\mu_{\mathrm{ES}} = 4$	
Relaxation time from SCH to WL	$7\ \mathrm{ns} < \tau_{\mathrm{s}} < 20\ \mathrm{ns}$	Fit
Capture time from WL to ES	$\tau_{\mathrm{c0}} = 1$ ps	(Bogaart et al. 2005)
Capture time from ES to GS	$\tau_{\mathrm{d0}} = 1$ ps	(Bogaart et al. 2005)
Carrier escape time from WL to SCH	$\tau_{\mathrm{qe}} = 3$ ns	(Gioannini and Montrosset 2007)
Carrier recombination time in SCH	$\tau_{\mathrm{sr}} = 4.5$ ns	(Gioannini and Montrosset 2007)
Carrier recombination time in WL	$2\ \mathrm{ps} < \tau_{\mathrm{qr}} < 100\ \mathrm{ps}$	Fit
Carrier recombination time in ES and GS	$\tau_{\mathrm{r}} = 1$ ns	(Bogaart et al. 2005)
Quantum dot density	$\mathrm{N_D} = 3.1 \cdot 10^{10}\mathrm{cm}^{-2}$	(Anantathanasarn et al. 2006)
Number of QD layers	$\mathrm{N_W} = 5$	
Average active QD layer thickness	$\mathrm{H_{act}} = 1.4$ nm	
Total quantum dot area	$\mathrm{A_D} = 7 \cdot 10^{-4}\mathrm{cm}^2$	
Total wetting layer area	$\mathrm{A_{WL}} = 7 \cdot 10^{-4}\mathrm{cm}^2$	
Refractive index	$\mathrm{n_r} = 3.261$	
Optical confinement factor	$\Gamma = 0.06$	
Transition matrix elements	$\lvert \mathrm{P}^{\sigma}_{\mathrm{GS,ES}} \rvert^2 = 2.70 \cdot \mathrm{m_0} \cdot \mathrm{E_{GS,ES}}\,\mathrm{kg} \cdot \mathrm{eV}$	Fit (Sugawara et al. 2000)
Internal modal loss	$\alpha_{\mathrm{i}} = 10\mathrm{cm}^{-1}$	
Temperature	$T = 288$ K	
Number of QD sub groups	$N = 31$	
Number of spectral groups	$M = 31$	

are the transition matrix elements of the GS and ES recombination (Sugawara et al. 2000); B_{cv} the Lorentzian homogenous broadening function (Sugawara et al. 2000) with a $2\hbar\Gamma_{\mathrm{cv}}$ FWHM and E_m the recombination energy of the m-th spectral group. The total modal gain for each spectral group G_m could be calculated with:

$$G_m = \Gamma \sum_n \left(g_{mn_{GS}} + g_{mn_{ES}} \right) - \alpha_i, m = 0, 1, \ldots, M-1, \tag{10}$$

where Γ is the optical confinement factor and α_i the internal modal loss. All the values of the parameters used in the simulations are given in Table 1.

The number used for the FWHM of the inhomogeneous broadening Γ_0 is based on time resolved differential reflection spectroscopy measurements and photoluminescence (PL) measurements at 4.8K applied on similar QD (Bogaart et al. 2005). The FWHM of the homogeneous broadening $2\hbar\Gamma_{\mathrm{cv}}$ is not known from previous research. It is used to fit the spectral width of the simulations to the measured spectrum. The resulting 40 meV can to a certain extend be explained by the previous measurements (Bogaart et al. 2005). In these measurements the PL-spectrum at room temperature show a FWHM of 93 meV while at

4.8 K a FWHM of 41 meV is measured. The difference between these values comes from the homogeneous broadening. The effective density of states in the WL per unit area is given by: $\rho_{WLeff} = \left(m_{eWL} k_B T/\pi\hbar^2\right)$. The total carrier capture time is measured to be approximately 2.2ps (Bogaart et al. 2005). Based on these measurements the carrier capture time from WL to ES, τ_{c0}, and from ES to GS, τ_{d0}, are chosen to be 1ps to have a total carrier capture time from WL to GS of 2ps. The carrier recombination rate is set at 1ns based on previous measurements (Bogaart et al. 2005). The relaxation time from SCH to WL, τ_s, and the carrier recombination time in the WL, τ_{qr}, together give a limitation to the number of carriers that can relax to the QDs. These two time constants are unknown and have been fitted to match the simulation results to the measurements. In the table a range is given over which the time constants were changed. The carrier escape time from WL to SCH τ_{qe} and the carrier recombination time in the SCH τ_{sr} do not have a large influence on the gain. They are chosen to be 3ns and 4.5ns respectively (Gioannini and Montrosset 2007). The number of QD sub groups and the number of spectral groups is chosen to be 31 to limit the amount of calculation time. Increasing the number of subgroups and spectral groups does not influence the gain spectrum and so does not give extra information.

5 Simulations

There are two major effects in the QD material which can explain the blue shift in the gain spectrum. We will first discuss both effects, show theoretical simulation results from limited parameter fits on the QD model, illustrating the effect on the calculated small signal gain spectra and compare them. Note that the simulations of the two effects are purely hypothetical. The values are chosen to isolate a particular effect and make clear what influence it has on the shape of the gain spectrum.

The first and most commonly used explanation for the spectral shift with current density is based on the contribution of higher energy states in the quantum dots to the optical gain. Carriers which are captured in a dot relax to the lowest energy state which has a free position with a rate $(1 - P_{ESn,GSn})/\tau_{c0,d0}$. If the two positions in the ground state are occupied ($P_{ESn} = 1$), the carriers are not able anymore to relax to the GS and will fill the fourfold ES and if filled also other higher energy states. In the gain spectrum this means that at low injection current densities only a peak appears around the central GS wavelength. When the injection current density is increased, the GS start to be fully occupied and a second peak starts to appear at the central ES wavelength. Due to the separate transition energies of the GS and ES two peaks will appear one at the GS and one at the ES wavelength. At a certain injection current density the ES peak will take over the peak wavelength. If the GS and ES are too close to each other, the peaks will overlap and there will be no clear distinction between the GS and ES peak. We have tried to reproduce the shape of the experimental gain spectra assuming this is the dominant effect. That has been done by fixing the WL wavelength at 1,13 μm ($E_{WL} = 1.096$ eV) (this WL wavelength is a theoretical value to better explain the effect, in reality the WL has a lower transition energy). The central GS wavelength was fixed at 1,73 μm ($E_{GS} = 0.716$ eV) and the central ES wavelength at 1.63 μm ($E_{ES} = 0.760$ eV). These values gave the best similarity of simulations with the measured gain. Due to the large energy gap between E_{ES} and E_{WL} electron energy levels there is a low escape rate from the ES directly back to the WL. If a carrier is captured in a dot there is nearly no chance that it will be able to go to another dot via the WL due to re-excitation. All the dots will be filled equally and the gain contribution from the GS and the ES are proportional to the inhomogeneous dot size distribution. In Fig. 5a the contributions from the GS(solid) and

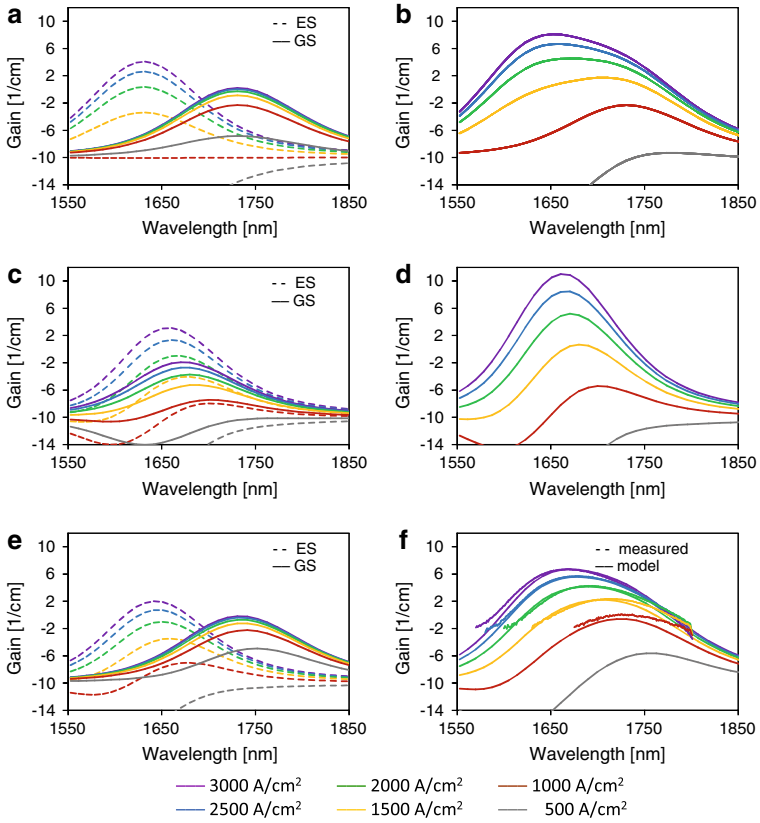

Fig. 5 Simulated gain spectra to show the different effects. Spectra are simulated for different injection current densities between 500 and 3,000 A/cm^2 in steps of 500 A/cm^2. In all figures the *lowest line* is the 500 A/cm^2 spectrum and the *upper line* the 3,000 A/cm^2 spectrum. On the *left* side **(a, c, e)** the spectra are split up in contribution from the GS (*solid*) and the ES (dashed) and on the *right* side **(b, d, f)** the total gain spectra are given. **(a, b)** Simulated modal gain spectra where the shift in peak wavelength is due to the shift from GS to ES. **(c, d)** Simulated modal gain spectra where the shift in peak wavelength is due to the dot size dependent filling due to dot size dependent escape rates. **(e, f)** Simulated modal gain spectra where the shift in peak wavelength is due to both effects. In **(f)** also the measured modal gain is given (*dashed*)

ES(dashed) to the total gain, Fig. 5b, are given for different injection current densities. First the GS starts to contribute to the gain and with increasing injection current density also the ES starts to contribute to the gain and takes over the peak wavelength.

The second effect in the QD material which can explain the blue shift in the gain spectrum is based on a dot-sized dependent escape rate from carriers in the dots to the wetting layer. The smaller dots have relatively high electron energy level which is closer to the electron energy level of the WL than the electron energy levels of large dots. The rate $1/\tau_{eESn}$ in (7) at which the carriers escape from the dots to the WL is larger for the smaller dots compared to the large dots due to the smaller energy differences. The relaxation time τ_c from the WL to the dots is however not energy level dependent which means that all dots will be filled at the same rate assuming that there are enough free states. The large dots will therefore be populated more and these dots also start to contribute to the gain at first time. When the

injection current density is increased also the smaller dots will be more populated with carriers and start to contribute to the gain. So the large dots first start to contribute to the gain in the longer wavelength region and while increasing the injection current density this shifts to the smaller dots which contributes to the gain in the shorter wavelength region. Again we have tried to reproduce the shape of the experimental gain spectra but now under conditions where the dot size dependent depopulation is the dominant effect. To simulate this we fixed the central GS wavelength at 1.66 μm ($E_{GS} = 0.746$ eV), the central ES wavelength at 1.64 μm ($E_{ES} = 0.755$ eV) and the WL wavelength at 1.54 μm ($E_{WL} = 0.805$ eV). Again these values are chosen to illustrate the effect, in reality we expect that the transition energy of the WL is higher and that the GS transition energy and the ES transition energy are more widely separated. In this case the different electron energy levels are close to each other and carriers can easily escape to a higher energy level due to the high escape rates $1/\tau_{eESn,GSn}$ and so switch to another dot via the wetting layer. The escape rate $1/\tau_{eESn}$ is still dependent on the ES electron energy level E_{ESn} in the dots (Eq. 7). Small dots have a relatively high energy level which increases the escape rate with respect to the large dots. In Fig. 5c the contribution from the GS(solid) and ES(dashed) to the total gain Fig. 5d are given for different injection current densities. In this figure one can see directly that at a certain injection current density part of the dots (long wavelengths) contribute to gain and another part still absorbs light.

6 Comparison with measurements

If we compare the two simulations with the measurement results we see that both optimized simulations do not follow the same trend as the measurements. In the first simulation we see that the peak wavelength starts at the GS wavelength and at a given moment switches to the ES wavelength, a kind of step function. This kind of step-like behavior from GS to ES gain is very familiar in InAs QD on GaAs substrate. In this material system the GS and ES do not overlap or only for a small part due to the inhomogeneous broadening. An extensive theoretical study has been done on this kind of behavior by Asryan et al. (2001). They also predict that the transition from GS to ES becomes more smooth if the GS peak and ES peak overlap more due to a smaller energy difference or a larger inhomogeneous broadening, for example the case in InAs QD on InP substrate. However our simulations show that this cannot be the only effect which causes the smooth transition from GS to ES gain.

The second simulation does have the continuously changing wavelength with respect to the injection current density like in the measurements, but the amount of peak wavelength shift is only 45 nm while the measurements show a shift of at least 65 nm. Besides the amount of shift of the peak wavelength, the spectral width is also not comparable with the measured gain spectra. The width of the gain spectrum from the GS is determined by the inhomogeneous broadening of the QD size, and is dependent on the homogeneous broadening. Gain from only one state in the QDs or from two states which are very close to each other like in the second simulation, does not give the same spectral width as measured given the 41 meV FWHM of the inhomogeneous broadening and the 40 meV FWHM of the homogeneous broadening.

In order to have a satisfactorily agreement between the simulation and the experiment a third simulation is presented where we did choose the location of the GS, the ES and the WL in such way that both effects are involved. In this simulation the GS wavelength is located at 1.73 μm ($E_{GS} = 0.716$ eV), the ES at 1.63 μm ($E_{ES} = 0.760$ eV), and the WL at 1.47 μm ($E_{WL} = 0.843$ eV). If we now take a look in Fig. 5e at the contributions from the GS(solid) and the ES(dashed) to the total gain at different injection current densities, we see that at

low injection current densities the coupling to the WL has a dominant effect on the peak wavelength of the gain. This coupling shifts the peak wavelength to longer wavelengths than the central GS wavelength at low injection current densities. This also explains the peak wavelength of 1.78 μm in the measured ASE spectrum at an injection current density of 500 A/cm^2 if we assume that the peak in the ASE spectrum corresponds to the peak in the gain spectrum. At higher injection current densities, the contribution to the gain from the ES forces the peak wavelength to the shorter wavelength region. In the contribution of the ES the influence of the coupling to the WL can still be seen which shifts the peak wavelength of the ES contribution to longer wavelengths, if the injection current density is decreased. The total gain is shown in Fig. 5f together with the measured gain. From this figure we clearly see the simulated gain spectra following the same trend as the measured gain spectra. We expect that the two mechanisms both shift the peak wavelength of the gain spectrum to even shorter wavelengths if there are other higher energy states available in the dots between the ES and the WL. The amount of shift originating from these higher energy states will decrease with respect to the increasing injection current densities due to the increasing number of states per energy range (Holm and Pistol 2002).

From the simulations we also noticed that the relaxation time from SCH to WL τ_s and the carrier recombination time in the WL τ_{qr} do not have influence on the change in shape of the gain spectrum, but only on the transparency current density of the GS and ES gain. The value for the transition matrix element determined in the fitting procedure corresponds to a spontaneous emission lifetime of 2.5ns which is compatible with a total carrier recombination time of 1ns for the GS and ES levels.

7 Conclusion

In this paper/letter we have presented the measured modal gain spectrum from the InAs/InP (100) QD gain material designed to emit light in the 1.60–1.80 μm wavelength region. The data have been measured using the ASE signals from a series of amplifiers with varying length, a method that can provide accurate data over a wide range of current densities of samples that are several millimeters or more long. The origin of the observed blue shift in this gain spectrum with increasing current, and the spectral width has been analyzed by modeling the QD gain material with a QD rate-equation model. The simulations show that the large blue shift is a combination of two effects which are present in the material. First the shift from GS to ES with respect to the injection current density and secondly the dot size dependent escape rates from the ES to the WL which decreases the gain for the short wavelengths and increases the gain for the long wavelengths. The latter effect is dominant at lower current densities. This knowledge of the behavior of the amplifier under different injection current densities can be used to optimize an integrated optical QD amplifier by e.g. the use of two section amplifiers biased at different injection current densities.

Acknowledgements This work is supported by the IOP (Innovatiegerichte Onderzoeksprogramma's) Photonic Devices program managed by the Technology Foundation STW (Stichting Technische Wetenschappen) and SenterNovem.

Open Access This article is distributed under the terms of the Creative Commons Attribution Noncommercial License which permits any noncommercial use, distribution, and reproduction in any medium, provided the original author(s) and source are credited.

References

Allen, C.Nì., Poole, P.J., Marshall, P., Fraser, J., Raymond, S., Fafard, S.: InAs self-assembled quantum-dot lasers grown on (100) InP. Appl. Phys. Lett. **80**(19), 3629–3631 (2002)

Anantathanasarn, S., Nötzel, R., van Veldhoven, P.J., van Otten, F.W.M., Barbarin, Y., Servanton, G., de Vries, T., Smalbrugge, B., Geluk, E.J., Eijkemans, T.J., Bente, E.A.J.M., Oei, Y.S., Smit, M.K., Wolter, J.H.: Lasing of wavelength-tunable (1.55 μm region) InAs/InGaAsP/InP (100) quantum dots grown by metal organic vapor-phase epitaxy. Appl. Phys. Lett. **89**(7), 073115 (2006)

Asryan, L.V., Grundmann, M., Ledentsov, N.N., Stier, O., Suris, R.A., Bimberg, D.: Effect of exited-state transitions on the threshold characteristics of a quantum dot laser. IEEE J. Quantum Electron. **37**(3), 418–425 (2001)

Barbarin, Y., Bente, E.A.J.M., Servanton, G., Mussard, L., Oei, Y.S., Nötzel, R., Smit, M.K.: Gain measurements of Fabry-Perot InP/InGaAsP lasers using an ultrahigh-resolution spectrometer. Appl. Optics. **45**(35), 9007–9012 (2006)

Bente, E.A.J.M., Smit, M.K.: Ultrafast InP optical integrated circuits. SPIE Proc. 6124 Optoelectronic Integrated Circuits VIII, Photonics West 2006, San Jose (2006)

Bogaart, E.W., Nötzel, R., Gong, Q., Haverkort, J.E.M., Wolter, J.H.: Ultrafast carrier capture at room temperature in InAs/InP quantum dots emitting in the 1.55 μm wavelength region. Appl. Phys. Lett. **86**(17), 173109 (2005)

Borri, P., Langbein, W., Hvam, J.M., Heinrichsdorff, f., Mao, M.H., Bimberg, D.: Ultrafast gain dynamics in InAs-InGaAs quantum-dot amplifiers. IEEE Phot. Technol. Lett. **12**(6), 594–596 (2000)

Caroff, P., Paranthoen, C., Platz, C., Dehaese, O., Folliot, H., Bertru, N., Labbé, C., Piron, R., Homeyer, E., Le Corre, A., Loualiche, S.: High-gain and low threshold InAs quantum-dot lasers on InP. Appl. Phys. Lett. **87**(7), 243107 (2005)

Fercher, A.F., Drexler, W., Hitzenberger, C.K., Lasser, T.: Optical coherence tomography—principles and applications. Rep. Prog. Phys. **66**, 239–303 (2003)

Gioannini, M., Montrosset, I.: Numerical analysis of the frequency chirp in quantum-dot semiconductor lasers. IEEE J. Quantum Electron. **43**(10), 941–949 (2007)

Gong, Q., Nötzel, R., Velthoven, P.J., van Eijkemans, T.J., Wolter, J.H.: Wavelength tuning of InAs quantum dots grown on InP (100) by chemical-beam epitaxy. Appl. Phys. Lett. **84**(2), 275–277 (2004)

Grillot, F., Veselinov, K., Gioannini, M., Montrosset, I., Even, J., Piron, R., Homeyer, E., Loualiche, S.: Spectral analysis of 1.55-μm InAs-InP(113)B quantum-dot lasers based on a multi-population rate equations model. IEEE J. Quantum Electron. **45**(7), 872–878 (2009)

Hakki, B.W., Paoli, T.L.: Gain spectra in GaAs double-heterostructure injection lasers. J. Appl. Phys. **46**(3), 1299–1306 (1975)

Holm, M., Pistol, M.E, Pryor, C.: Calculations of the electronic structure of strained InAs quantum dots in InP. J. Appl. Phys. **92**(2), 932–936 (2002)

Liu, G., Stintz, A., Li, H., Malloy, K.J., Lester, L.F.: Extremely low room-temperature threshold current density diode lasers using InAs dots in $In_{0.15}Ga_{0.85}As$ quantum well. IEEE Electron. Lett. **35**(14), 1163–1165 (1999)

Miska, P., Even, J., Marie, X., Dehaese, O.: Electronic structure and carrier dynamics in InAs/InP double-cap quantum dots. Appl. Phys. Lett. **94**, 061919 (2009)

Nötzel, R., Anantathanasarn, S., van Veldhoven, R.P.J., van Otten, F.W.M., Eijkemans, T.J., Trampert, A., Satpati, B., Barbarin, Y., Bente, E.A.J.M., Oei, Y.S., de Vries, T., Geluk, E.J., Smalbrugge, B., Smit, M.K., Wolter, J.H.: Self assembled InAs/InP quantum dots for telecom applications in the 1.55 μm wavelength range: wavelength tuning, stacking, polarization control, and lasing. Jpn. J. Appl. Phys. **45**(8B), 6544–6549 (2006)

Oster, A., Erbert, G., Wenzel, H.: Gain spectra measurements by a variable strip length method with current injection. IEEE Electron. Lett. **33**(10), 864–866 (1997)

Rosenbrock, H.H.: Some general implicit processes for the numerical solution of differential equations. Computer. J. **5**(4), 329–330 (1963)

Rossetti, M., Bardella, P., Montrosset, I.: Numerical investigation of power tunability in two-section QD superluminescent diodes. Opt. Quant. Electron. **40**(14–15), 1129–1134 (2008)

Sugawara, M., Mukai, K., Nakata, Y.: Light emission spectra of columnar-shaped self-assembled InGaAs/GaAs quantum-dot lasers: Effect of homogeneous broadening of the optical gain on lasing characteristics. Appl. Phys. Lett. **74**(11), 1561–1563 (1999)

Sugawara, M., Mukai, K., Nakata, Y., Ishikawa, H.: Effect of homogeneous broadening of optical gain on lasing spectra in self-assembled $In_xGa_{1-x}As$/GaAs quantum dot lasers. Phys. Rev. B **61**(11), 7595–7603 (2000)

Thomson, J.D., Summers, H.D., Hulyer, P.M., Blood, P.: Determination of single-pass optical gain and internal loss using a multisection device. Appl. Phys. Lett. **75**(17), 2527–2529 (1999)

Wang, H., Yuan, J., van Veldhoven, P.J., de Vries, T., Smalbrugge, B., Geluk, E.J., Bente, E.A.J.M., Oei, Y.S., Smit, M.K., Anantathanasarn, S., Nötzel, R.: Butt joint integrated extended cavity InAs/ InP (100) quantum dot laser emitting around 1.55 μm. IEEE Electron. Lett. **44**(8), 522–523 (2008)

Werle, P.: A review of recent advances in semiconductor laser based gas monitors. Spectrochimica Acta Part A **54**(2), 197–236 (1998)

Xin, Y.C., Martinez, A., Saiz, T., Moscho, A.J., Li, Y., Nilsen, T.A., Gray, A.L., Lester, L.F.: 1.3-μm quantum-dot multisection superluminescent diodes with extremely broad bandwidth. IEEE Phot. Technol. Lett. **19**(7), 501–503 (2007)